ChemComm

COMMUNICATION

View Article Online
View Journal | View Issue

Cite this: *Chem. Commun.*, 2022, **58**, 11689

Received 12th July 2022,
Accepted 23rd September 2022

DOI: 10.1039/d2cc03875g

rsc.li/chemcomm

In situ excitation of BODIPY fluorophores by ^{89}Zr-generated Cerenkov luminescence†

Katie Gristwood,[a] Saimir Luli,[b] Kenneth S. Rankin[c] and James C. Knight *[a]

Secondary Cerenkov-induced fluorescence imaging (SCIFI) is an emerging optical imaging technology that affords high signal-to-noise images by utilising radionuclide-generated Cerenkov luminescence to excite fluorescent probes. BODIPY dyes offer attractive properties for SCIFI, including high quantum yields and photochemical stability, yet their utility in this application in combination with clinically relevant β$^+$-emitting radioisotopes remains largely unexplored. In this report, the fluorescence properties of three *meso*-substituted BODIPY analogues have been assessed in combination with the positron emitter zirconium-89. Most notably, SCIFI data acquired over 7 days shows the BODIPY scaffold remain largely inert to radiolysis, indicating the promising utility of this fluorophore class in SCIFI applications.

Cerenkov luminescence (CL) is generated by charged particles traveling faster than the speed of light through a dielectric medium.[1,2] In recent years, CL has shown promising utility in several medical applications, including image-guided surgery,[3] radiotherapy dosimetry,[4] and activation of photodynamic therapies.[5] Examples of non-medical CL-based applications in radiosynthesis,[6] microfluidics[7] and plant sciences[8] are also emerging. However, the poor penetrance of this low-intensity, blue-weighted light, particularly in biological tissues, limits the scope of this technique.[9] More recently, secondary Cerenkov-induced fluorescence imaging (SCIFI; also known as Cerenkov Radiation Energy Transfer [CRET]) has emerged offering image acquisition at greater depths by using CL to excite secondary fluorophores with more penetrating emissions, obviating the need for conventional externally-applied excitation sources which are limited by autofluorescence, reflection, and scatter.

SCIFI was first reported in 2010 by Liu *et al.* who observed CL-induced fluorescence following subcutaneous and intramuscular co-injection of ^{131}I (β$^-$ emitter) and near-infrared quantum dots (QD655) in mice.[10] Subsequently, a limited selection of fluorophore and radioisotope combinations have been evaluated in SCIFI investigations, including a study by Dothager *et al.* that applied ^{64}Cu- and ^{18}F-generated CL to excite Qtracker705 quantum dots in a subcutaneous pseudotumour mouse model.[11] Later, Thorek *et al.* used ^{18}F-generated CL to excite fluorescein in an *in vivo* subcutaneous capillary model and observed a 5.7-fold higher signal-to-noise ratio for SCIFI compared to standard fluorescence. This study also evaluated the *in vivo* colocalization of ^{89}Zr-DFO-trastuzumab and cyclic-RGD QD605 in HER2+ tumour xenografts in mice, culminating in SCIFI images of $\alpha_v\beta_3$ in the tumour microenvironment with low background relative to that obtainable by external excitation.[1]

Boron-dipyrromethene (BODIPY) fluorophores are attractive candidates for SCIFI due to their high quantum yields, excellent photostability, and tuneable spectroscopic properties.[12,13] BODIPY dyes are also typically insensitive to environmental conditions, such as polarity and pH.[13] Notably, the nature of substituents around the BODIPY core can significantly influence its fluorescent properties. For instance, alkyl substitution at alpha and beta positions typically results in a slight bathochromic shift in emission maxima compared to unsubstituted analogues,[14] while more pronounced effects are commonly observed upon *meso*-substitution of the BODIPY core.[15] Leen *et al.* found that the addition of a cyano group at the *meso*-position results in a drastic bathochromic shift and, in contrast, heteroatomic *meso*-substituents (*e.g.* amines, ethers) lead to hypsochromic shifts.[16] Similar effects have been observed with other *meso*-substituted BODIPYs according to the electronic character of the substituent, however it is worth noting several exceptions to this trend which indicate the additional influence of other substituent properties.

Recently, Genovese *et al.* doped Pluronic–silica nanoparticles with five different fluorophores, including a BODIPY dye, and combined these with the β$^-$–emitting radiopharmaceutical agent

[a] *School of Natural and Environmental Sciences, Faculty of Science, Agriculture and Engineering, Newcastle University, Newcastle Upon Tyne, NE1 7RU, UK. E-mail: James.Knight2@newcastle.ac.uk, k.gristwood2@newcastle.ac.uk*
[b] *Institute of Cellular Medicine, Faculty of Medical Sciences, Newcastle, Newcastle Upon Tyne, NE2 4HH, UK. E-mail: saimir.luli@newcastle.ac.uk*
[c] *Translational and Clinical Research Institute, Faculty of Medical Sciences, Newcastle University, Newcastle Upon Tyne, NE2 4HH, UK. E-mail: kenneth.rankin@newcastle.ac.uk*

† Electronic supplementary information (ESI) available: Further methodological information, supplementary emission spectra and ^{89}Zr decay curve and half-life. See DOI: https://doi.org/10.1039/d2cc03875g

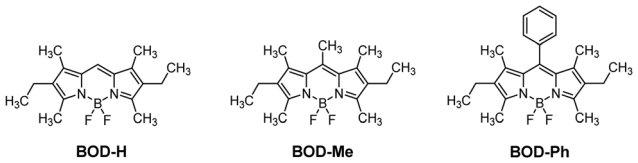

Fig. 1 Structures of the BODIPY compounds used in this study.

^{32}P-ATP, leading to the conversion of CL to near-infrared light *via* an efficient series of energy transfer processes.[17] To the best of the authors' knowledge, BODIPY dyes have not previously been used in combination with positron (β^+)-emitting isotopes for SCIFI, whereas the broad utility of clinically-relevant positron emitters in this application has been well-established with other fluorophores.[1]

In this report, we have examined three BODIPY analogues derived from {3-ethyl-5-[(4-ethyl-3,5-dimethyl-2*H*-pyrrol-2-ylidene)-methyl]-2,4-dimethyl-1*H*-pyrrolato-1,N5}difluoroboron (Fig. 1) differing only by the substituent at the *meso*-position to investigate the suitability of the BODIPY scaffold for SCIFI. The BODIPYs included in this investigation are referred to hereafter as BOD-H (hydrogen/unsubstituted), BOD-Me (methyl) and BOD-Ph (phenyl). The positron-emitting radiometal ^{89}Zr was selected as the source of CL on the basis of its emerging clinical utility and recent validation in CL-based imaging studies,[18–21] and relatively long half-life ($t_{1/2}$ = 78.4 h) for multi-day evaluation which is not possible with shorter-lived alternatives (*e.g.* ^{18}F: $t_{1/2}$ = 109.8 min). Furthermore, while the positron yield of ^{89}Zr (22.7%) is low compared to more commonly used PET radioisotopes (*e.g.* ^{18}F: 100%), the mean β^+ emission energy and Cerenkov photon yield (CPY) of ^{89}Zr ($E_{\beta+}$ = 395.5 keV; CPY = 2.29) are relatively high (*e.g.* ^{18}F: $E_{\beta+}$ = 249.8 keV; CPY = 1.32).[22]

A partial CL emission spectrum for ^{89}Zr was generated between 500 and 840 nm (20 nm increments) using an optical *in vivo* imaging system (IVIS) (Fig. 2). The solution was prepared by diluting ^{89}Zr (10.8 MBq) in 1 M oxalic acid with phosphate-buffered saline (PBS; pH 7.4, 100 μL, 0.108 MBq μL^{-1}) in a black wall clear-bottom 96-well plate. The resulting emission profile, measured as total photon flux (photons per second; p/s), is consistent with a previously reported ^{89}Zr-generated CL spectrum acquired under different conditions.[23] The spectral range of the IVIS emission filters does not extend to the CL maximum emission peak in the UV-blue region (<500 nm), however the broad emission profile of ^{89}Zr-generated CL lends it wide-ranging utility as an excitation source.

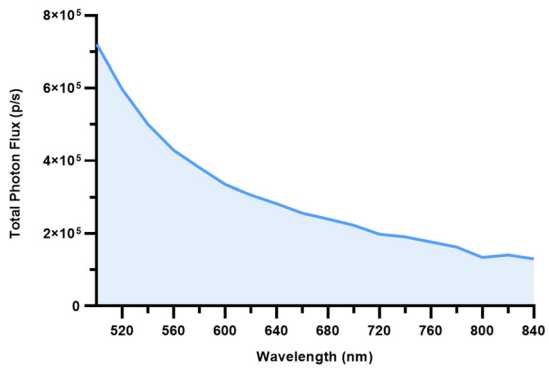

Fig. 2 Cerenkov luminescence spectrum of ^{89}Zr-oxalate in PBS.

The fluorescence properties of each BODIPY dye were first assessed by conventional external light excitation (Fig. 3A–C). The water-insoluble BODIPY dyes were dissolved in dimethyl sulfoxide (DMSO) which has a relatively high permittivity (ε_r = 46.6)[24] and refractive index (n = 1.477)[25] that renders this solvent well-suited to SCIFI investigations. Absorbance spectra between 440–680 nm (0.5 nm increments) were acquired on a Nanodrop One^C and fluorescence emission spectra were acquired by IVIS imaging with an 465 nm excitation filter and emission measured between 500–660 nm (20 nm increments; [BODIPY] = 1 mM). Additional high-resolution laser-excited fluorescence spectra were acquired with a spectrofluorophotometer (Fig. S1, ESI†). The BODIPY dye absorbance and emission maxima were measured as follows: BOD-H $\lambda_{abs/em}$ = 528/540 nm; BOD-Me: $\lambda_{abs/em}$ = 518/543 nm; BOD-Ph $\lambda_{abs/em}$ = 526/540 nm.

Thereafter, an equivalent series of each BODIPY dye ([BODIPY] = 1 mM in DMSO) was combined with ^{89}Zr (0.25 MBq), and CL-induced BODIPY fluorescence was measured by IVIS imaging with excitation light blocked (Fig. 3D–F). Promisingly, this approach enabled rapid (<5 min) acquisition of emission spectra for all three BODIPYs without the need for an external light excitation source. This data is largely consistent with the spectral signature of the BODIPY dyes acquired under specific excitation and emission filters. A steeper profile is seen in the higher energy portion of the CL-induced emission spectra which is attributable to the spectral unmixing process. The absence of signal <520 nm in the emission spectra generated from ^{89}Zr-containing BODIPY-free control wells reflects the CL energy

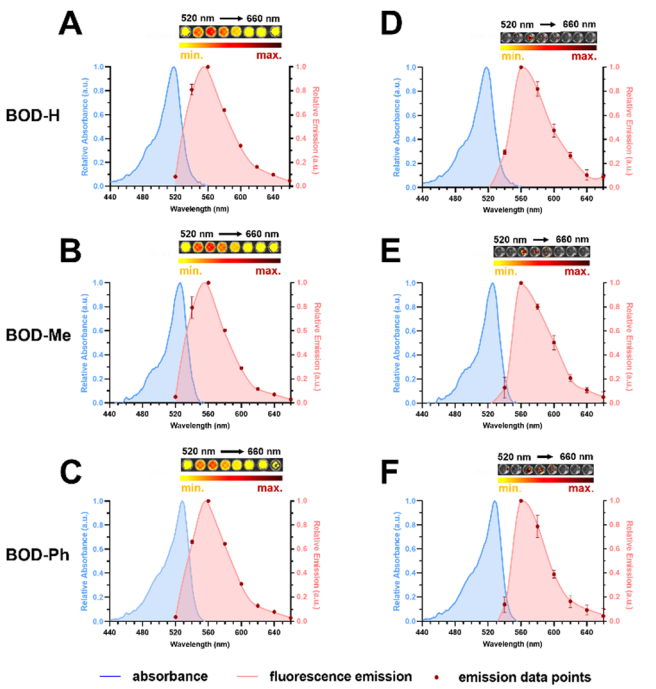

Fig. 3 BOD-H, BOD-Me and BOD-Ph absorption (blue) and fluorescence emission (red) spectra in DMSO. (A–C) Fluorescence spectra obtained by external light excitation (465 nm) of 1 mM BODIPY in DMSO. (D–F) Fluorescence spectra obtained by Cerenkov luminescence excitation of 1 mM BODIPY in DMSO containing ^{89}Zr (0.25 MBq).

transfer to each BODIPY. Lastly, CL-induced fluorescence signal was considerably lower than obtained by light excitation for each BODIPY (Fig. 3A–F; inset well-plate images), although it remained well-within the sensitivity range of the IVIS system.

To explore the relationship between BODIPY concentration and CL (based on ^{89}Zr activity), serial dilutions of each BODIPY dye ranging from 1 mM to 10 μM were combined with aliquots of ^{89}Zr-oxalate (0.25 MBq; 0.05 MBq μL^{-1}) to a final volume of 100 μL in DMSO, and SCIFI images were acquired using the IVIS. The excitation light was blocked and fluorescence emissions between 500–660 nm, as well as open filter, were measured. Net photon flux was calculated by subtracting the average total flux of the ^{89}Zr-DMSO wells from the total flux of each well in the BODIPY serial dilution containing ^{89}Zr, therefore omitting the contribution of the ^{89}Zr-generated Cerenkov luminescence and leaving only the SCIFI signal. Plots of the average net photon flux values against BODIPY dye concentration (Fig. 4) reveal a hyperbolic relationship in which fluorescence intensity reaches a plateau toward higher BODIPY concentrations, representing the maximum fluorescence threshold attainable by the number of CL photons generated by ^{89}Zr in these conditions. Dothager *et al.* reported an analogous effect and similarly attributed this relationship to the low intensity nature of CR and the high molar absorptivity of Qtracker705.[11] In addition, a SCIFI study investigating luminescent lanthanide complexes comprising of terbium(III) and the radioisotopes ^{18}F and ^{89}Zr also described a comparable non-linear relationship between concentration and fluorescence intensity.[26] External light excitation of the BODIPY dyes yielded significantly higher photon fluxes (Fig. 3A–C) which remained linear correlated with dye concentration (Fig. S3, ESI†), supporting this hypothesis.

Lastly, in order to gauge the sensitivity of the BODIPY dyes to radiolysis caused by prolonged co-incubation with ^{89}Zr, we measured the net photon flux for each BODIPY dye over the course of 7 days using a range of ^{89}Zr activity : [BODIPY] ratios from 0.25 : 1 to 25 : 1 kBq μM^{-1} (Fig. 5; full range tabulated data in Tables S1–S3, ESI†). Method validation involved longitudinal analysis of the total flux of ^{89}Zr-only control wells which adhered to a exponential one-phase radioactive decay model (R^2 = 0.98) consistent with previous reports.[18] The decay half-life of ^{89}Zr was calculated as 78.3 ± 6.9 h which is in good agreement with the widely reported value of 78.41 h (Fig. S2, ESI†). Thereafter, calculations of the theoretical photon flux values for each BODIPY at each time point, based solely on photon flux values at the start of the experiment and the known physical decay characteristics of ^{89}Zr, were performed to provide reference data (Fig. 5: blue lines). Inspection of the experimental data (Fig. 5: red lines) reveals close alignment with these theoretical values for all conditions, with the exception of a 52.3 ± 23.2% reduction in SCIFI signal for BOD-Me at 168 h that counterintuitively occurred at the lowest ^{89}Zr/kBq to [BODIPY]/μM ratio (0.25 : 1). In contrast, both BOD-H and BOD-Ph remained inert to radiolysis for the duration of the experiment, even at the highest ^{89}Zr : [BODIPY] ratios, indicating a promising ability to remain functional in SCIFI investigations for at least 7 days. Increasing ^{89}Zr activity up to 10 : 1 kBq μM^{-1} with a constant BODIPY concentration of 150 μM further verified the stability of these dyes (Fig. S4 and Table S4, ESI†). While the complex effects of substitution upon the intrinsic properties of BODIPY dyes

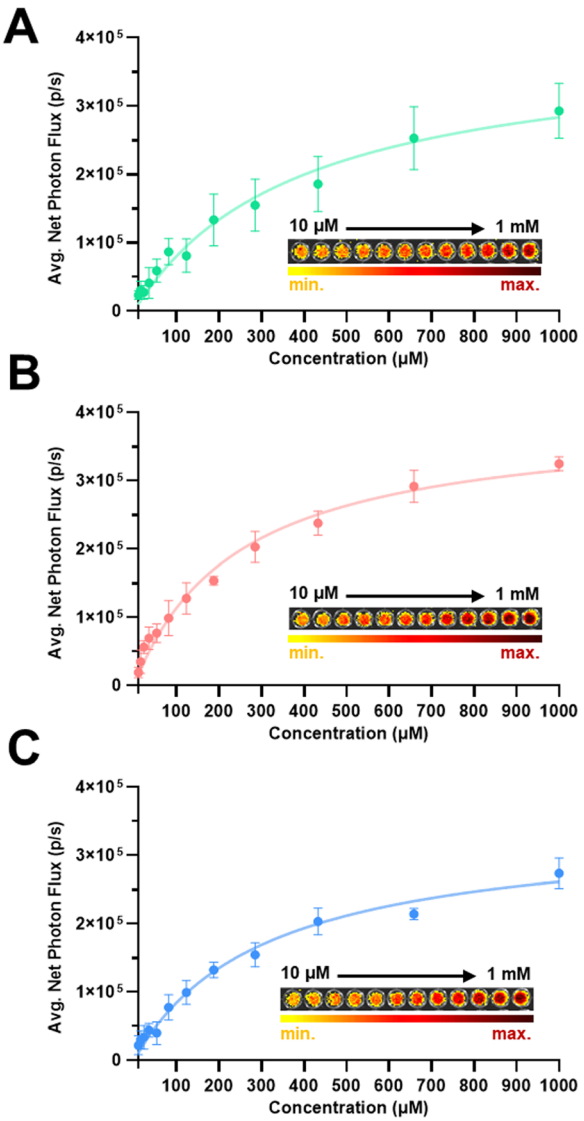

Fig. 4 SCIFI intensity against BODIPY concentration; (A) BOD-H, (B) BOD-Me, (C) BOD-Ph. Aliquots of ^{89}Zr (0.25 MBq) were added to serial dilutions (10 μM to 1 mM; DF= 1.5199) of each BODIPY dye. Net photon flux (p/s) [dots] measurements were taken with an open filter and the non-linear data was fitted to a hyperbola curve. IVIS images of the wells are shown in inset panels, and are normalised to the maximum photon flux (p/s) value. Error bars = SEM.

is a relatively young field of study, the impact of methyl substitution upon BODIPYs has been the focus of a computational study by Mukherjee *et al.* in 2015 which reported significant effects upon of the photophysical properties and stability of BODIPY dyes.[27] Moreover, a study by Hinkeldey *et al.* that measured the photostability of a small panel of BODIPY derivatives with comparable *meso*-substitution, found a methyl-substituted derivative to have lower photostability than phenyl-substituted and unsubstituted analogues,[28] consistent with the variation observed in this study.

In summary, this study is an informative first step in the evaluation of BODIPYs as secondary fluorophores in SCIFI applications involving positron-emitting isotopes. From the data described herein, BODIPYs appear to represent promising candidates for this emerging optical imaging modality, despite some

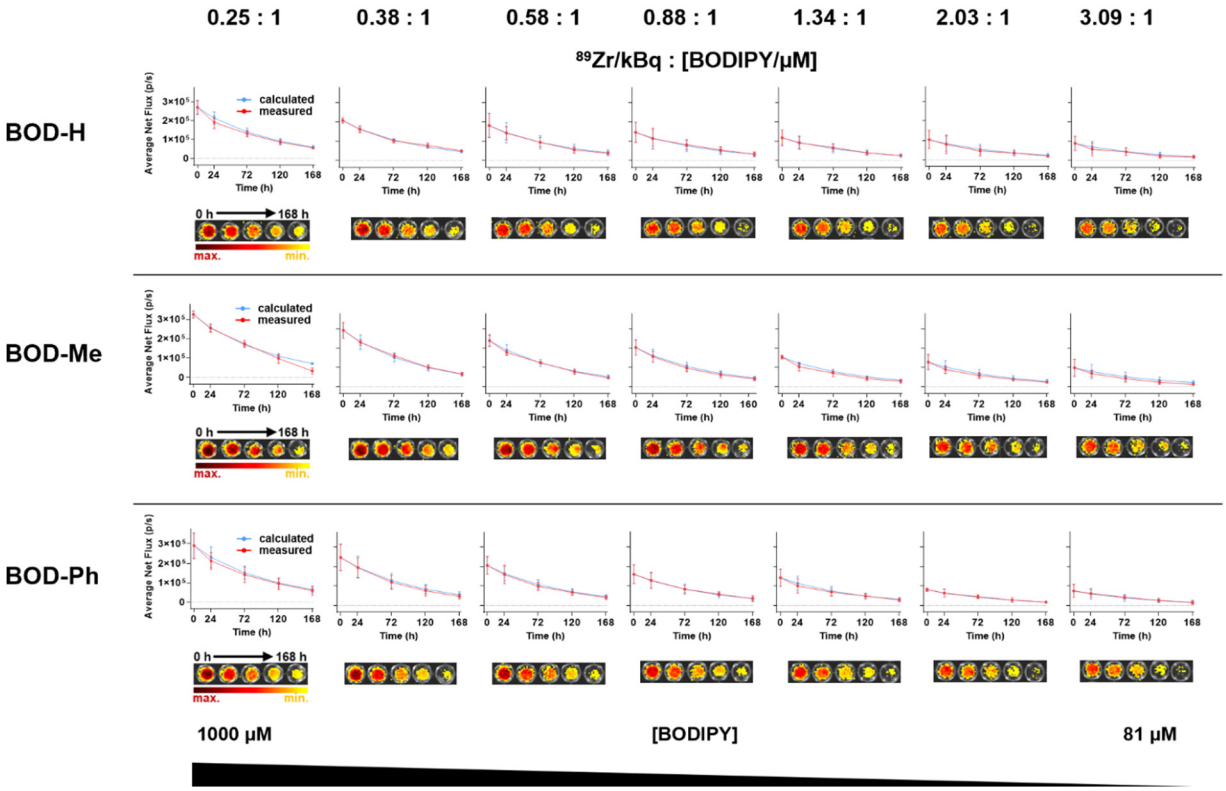

Fig. 5 Monitoring SCIFI intensity over 168 h at varying ^{89}Zr (kBq):[BODIPY] (μM) ratios for BOD-H, BOD-Me and BOD-Ph. Net photon flux (p/s) values (red lines) were measured at 0, 24, 72, 120, and 168 h after addition of ^{89}Zr (0.25 MBq) to serial dilutions of each BODIPY dye (1000–10 μM; DF = 1.5199) using an open filter; see supplementary Tables S1–S3 (ESI†) for full range tabulated data. Theoretical net photon flux (p/s) values (blue lines) were calculated based on the net photon flux (p/s) value for each BODIPY at 0 h and the decay half-life of ^{89}Zr. The ^{89}Zr (kBq) : [BODIPY] (μM) ratios are shown above each dilution. Error bars = SEM. Inset images show representative open filter IVIS images of sample wells for each BODIPY concentration at 0, 24, 72, 120, and 168 h.

substituent-dependant variability in stability. Encouraged by these findings, we are now exploring the SCIFI utility of more elaborate BODIPY motifs with larger Stokes shifts resulting in near-infrared emissions that are of greater biomedical relevance.

Conflicts of interest

There are no conflicts to declare.

Notes and references

1 D. L. Thorek, A. Ogirala, B. J. Beattie and J. Grimm, *Nat. Med.*, 2013, **19**, 1345–1350.
2 D. L. Thorek, R. Robertson, W. A. Bacchus, J. Hahn, J. Rothberg, B. J. Beattie and J. Grimm, *Am. J. Nucl. Med. Mol. Imaging*, 2012, **2**, 163–173.
3 C. Darr, N. Harke, J. P. Radtke, L. Yirga, C. Kesch, M. Grootendorst, W. Fendler, P. Fragoso Costa, C. Rischpler, C. Praus, J. Haubold, H. Reis, T. Hager, K. Herrmann, I. Binse and B. Hadaschik, *J. Nucl. Med.*, 2020, **61**, 1500–1506.
4 M. R. Ashraf, M. Rahman, R. Zhang, B. B. Williams, D. J. Gladstone, B. W. Pogue and P. Bruza, *Front. Phys.*, 2020, **8**, 328.
5 A. E. Spinelli and F. Boschi, *Front. Phys.*, 2021, **9**, 637120.
6 R. M. van Dam and A. F. Chatziioannou, *Front. Phys.*, 2021, **9**, 632056.
7 A. A. Dooraghi, P. Y. Keng, S. Chen, M. R. Javed, C.-J. C. Kim, A. F. Chatziioannou and R. M. van Dam, *Analyst*, 2013, **138**, 5654–5664.
8 K. Kurita, N. Suzui, Y.-G. Yin, S. Ishii, H. Watabe, S. Yamamoto and N. Kawachi, *J. Nucl. Sci. Technol.*, 2017, **54**, 662–667.
9 Y. Ni and J. Wu, *Org. Biomol. Chem.*, 2014, **12**, 3774–3791.
10 H. Liu, X. Zhang, B. Xing, P. Han, S. S. Gambhir and Z. Cheng, *Small*, 2010, **6**, 1087–1091.
11 R. S. Dothager, R. J. Goiffon, E. Jackson, S. Harpstrite and D. Piwnica-Worms, *PLoS One*, 2010, **5**, e13300.
12 A. Schmitt, B. Hinkeldey, M. Wild and G. Jung, *J. Fluoresc.*, 2009, **19**, 755–758.
13 A. Loudet and K. Burgess, *Chem. Rev.*, 2007, **107**, 4891.
14 A. B. Nepomnyashchii, S. Cho, P. J. Rossky and A. J. Bard, *J. Am. Chem. Soc.*, 2010, **132**, 17550–17559.
15 A. Prlj, A. Fabrizio and C. Corminboeuf, *Phys. Chem. Chem. Phys.*, 2016, **18**, 32668–32672.
16 V. Leen, P. Yuan, L. Wang, N. Boens and W. Dehaen, *Org. Lett.*, 2012, **14**, 6150–6153.
17 D. Genovese, L. Petrizza, L. Prodi, E. Rampazzo, F. De Sanctis, A. E. Spinelli, F. Boschi and N. Zaccheroni, *Front. Chem.*, 2020, **8**, 71.
18 A. Ruggiero, J. P. Holland, J. S. Lewis and J. Grimm, *J. Nucl. Med.*, 2010, **51**, 1123–1130.
19 J. P. Holland, G. Normand, A. Ruggiero, J. S. Lewis and J. Grimm, *Mol. Imaging*, 2011, **10**, 177.
20 A. Natarajan, F. Habte, H. Liu, A. Sathirachinda, X. Hu, Z. Cheng, C. M. Nagamine and S. S. Gambhir, *Mol. Imaging Biol.*, 2013, **15**, 468–475.
21 F. Habte, A. Natarajan, D. S. Paik and S. S. Gambhir, *Mol. Imaging*, 2018, **17**, DOI: 10.1177/1536012118788637.
22 J. Daouk, B. Dhaini, J. Petit, C. Frochot, M. Barberi-Heyob and H. Schohn, *Radiation*, 2021, **1**, 5–17.
23 Y. Zhao, T. M. Shaffer, S. Das, C. Pérez-Medina, W. J. M. Mulder and J. Grimm, *Bioconjugate Chem.*, 2017, **28**, 600.
24 M. S. Bakshi, J. Singh, H. Kaur, S. T. Ahmad and G. Kaur, *J. Chem. Eng. Data*, 1996, **41**, 1459–1461.
25 R. G. LeBel and D. A. I. Goring, *J. Chem. Eng. Data*, 1962, **7**, 100–101.
26 A. G. Cosby, S. H. Ahn and E. Boros, *Angew. Chem., Int. Ed.*, 2018, **57**, 15496–15499.
27 S. Mukherjee and P. Thilagar, *RSC Adv.*, 2015, **5**, 2706–2714.
28 B. Hinkeldey, A. Schmitt and G. Jung, *Chem. Phys. Chem.*, 2008, **9**, 2019–2027.

